Supplementary Information

Tailoring self-organized nanostructured morphologies in kilometer-long polymer fibre

Tural Khudiyev[1], Osama Tobail[1,2] & Mehmet Bayindir[1,3,4*]

[1]UNAM-National Nanotechnology Research Center, Bilkent University, 06800 Ankara, Turkey

[2]Egypt Nanotechnology Center, Cairo University, 12588 Cairo, Egypt

[3]Institute of Materials Science and Nanotechnology, Bilkent University, 06800 Ankara, Turkey

[4]Department of Physics, Bilkent University, 06800 Ankara, Turkey

*Correspondence and requests for materials should be addressed to M. B. (e-mail: bayindir@nano.org.tr).

Table of Contents

FDTD Simulations

Finite-difference time-domain (FDTD) simulations are performed by using commercial software (Lumerical Solutions Inc.) A total field scattered field (TFSF) source is used for illumination, as this source type yields a scattered field separate from the incident field and is therefore well-suited for scattering analysis. FDTD simulations are calculated in three dimensional simulation regions. Frequency-domain power monitors are used to collect scattered light. Material parameters, measured with a UV-Vis-NIR Ellipsometer, are inserted into simulations in Figure 5e. For theoretical investigation, constant refractive indices of 3.25 and 1.41 and negligible absorption are assumed for As_2Se_3 and PVDF, respectively, and utilized for the design of colored nanostructures. The use of real material parameters results in major decreases in scattering efficiency for smaller wavelengths, as the As_2Se_3 core absorbs strongly in this region.

Analytical Solutions

Analytical solutions for scattering from coated spheres are based on Lorenz-Mie formalism. Scattering efficiency for unpolarized light can be expressed as;

$$Q_{sca}(x) = \frac{1}{x}\sum_{n=-\infty}^{n=\infty}(|a_n|^2 + |b_n|^2)$$

$x = 2\pi a/\lambda$, where a is radius of the core and $y = 2\pi b/\lambda,$ where b is total radius of the core-shell sphere. Scattering coefficients (a_n and b_n) for coated sphere case and detailed information about solution procedures can be found in Ref. 1. Scattering plots can be constructed using the equation provided above, by taking real ellipsometric (*n*,*k*) values into account.

Scattering Measurements

Core-shell nanostructures are dispersed on glass and red, green and blue arrays of colored spheres are selected for characterization under dark field illumination of an inverted light microscope. Scattered light is collected by a MAYA spectrometer. Optical images of colored nanostructures are taken by a digital camera attached to the microscope.

[1] Bohren, C. F. & Huffman, D. R. Absorption and Scattering of Light by Small Particles (Wiley, 2008).

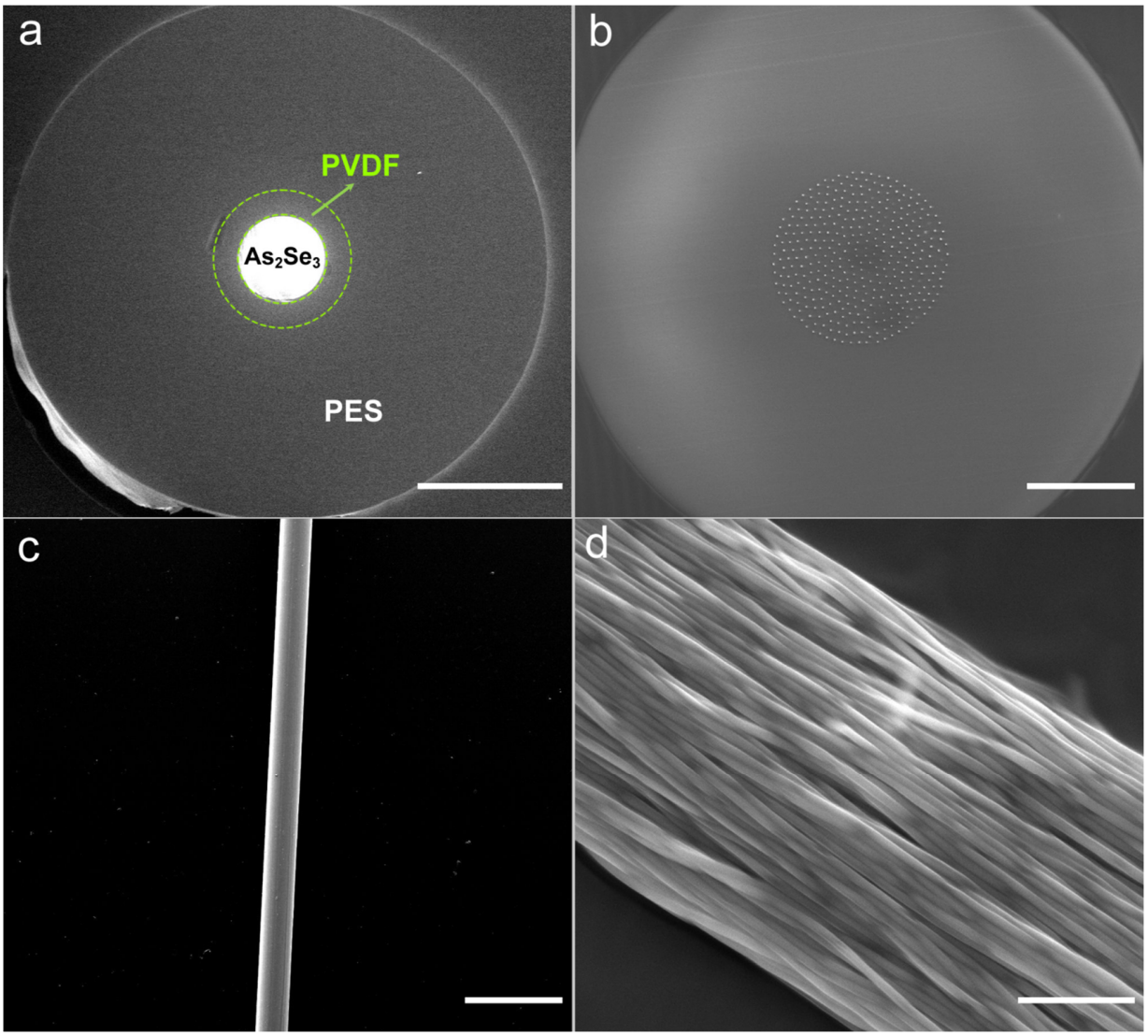

Figure S1| SEM images of step I and step II fibres. Cross-sectional images of **a,** step I (scale bar, 100 µm) and **b,** step II (scale bar, 50 µm) fibers obtained by a low temperature, multimaterial fibre drawing method. Free-standing nanostructures obtained by etching the PES sheath by DCM prior to SEM imaging. Longitudinal images of **c,** step I (scale bar, 250 µm) and **d,** step II (scale bar, 2 µm) micro- and nanostructures are also provided.

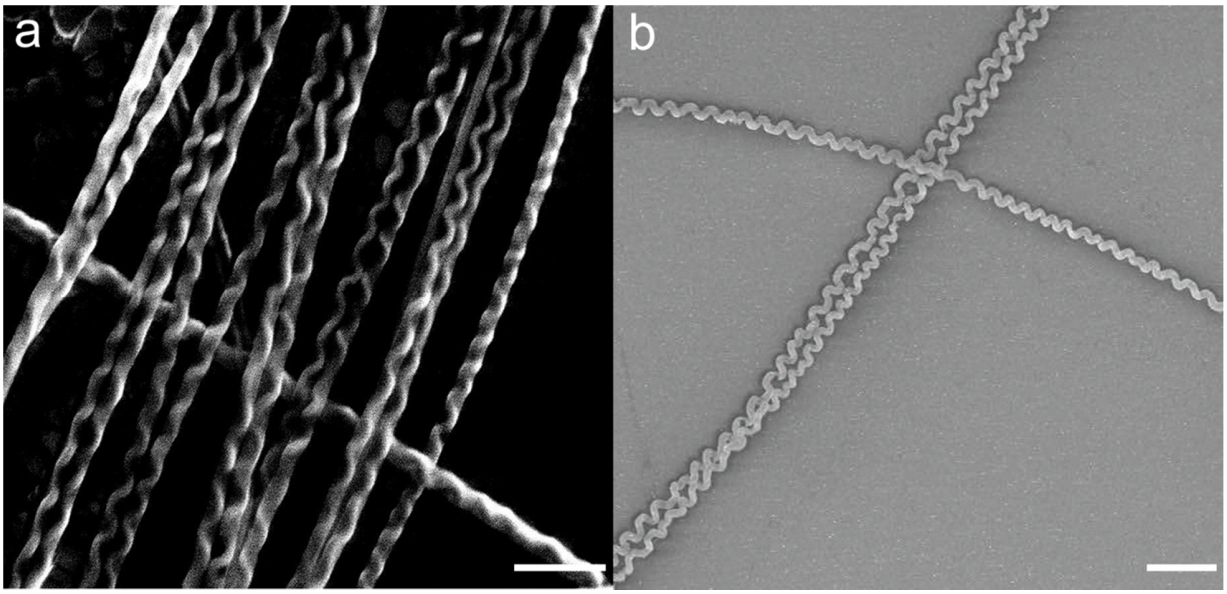

Figure S2| Core-only nanoschemes. In addition to core-shell nanoschemes, core-only structures can be obtained by removing the PVDF shell layer. We demonstrate this process by plasma etching an array of core-shell nanosprings, but etchant solvents or drawing core-only fibres may be utilized to the same effect. Scale bars, 5 μm.

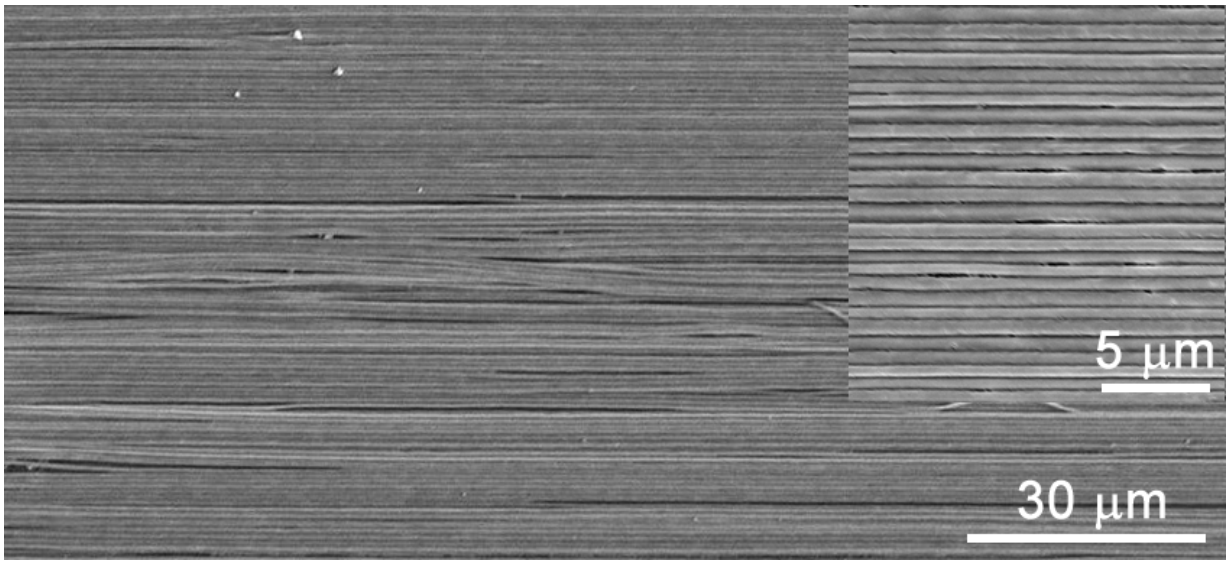

Figure S3 | Highly ordered single-layer nanostructure arrays. Second step in-fiber nanowires are self-aligned into parallel single-layer structures after dissolving the PES sheath region in DCM.

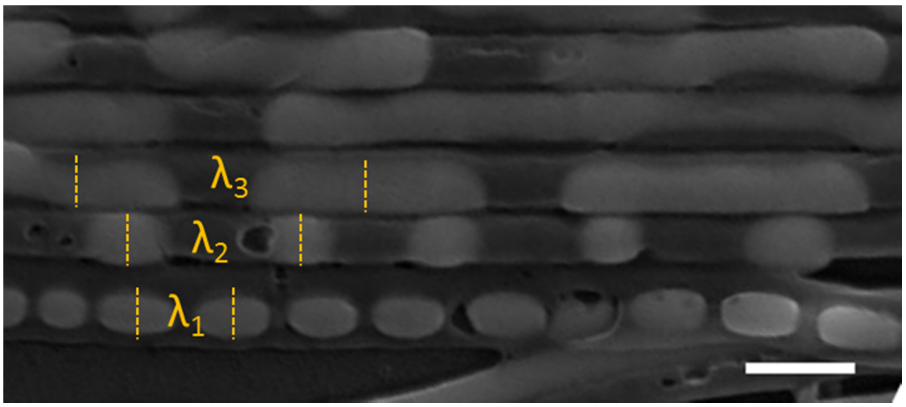

Figure S4| Adjustable structure parameters. Different processing times and temperatures result in changes in structure periods and lengths. Discrete rods with varying repetition length (λ_1=140 nm, λ_2=240 nm, λ_3=580 nm) are produced by exposing a nanowire array to a temperature gradient. Scale bar, 200 nm.

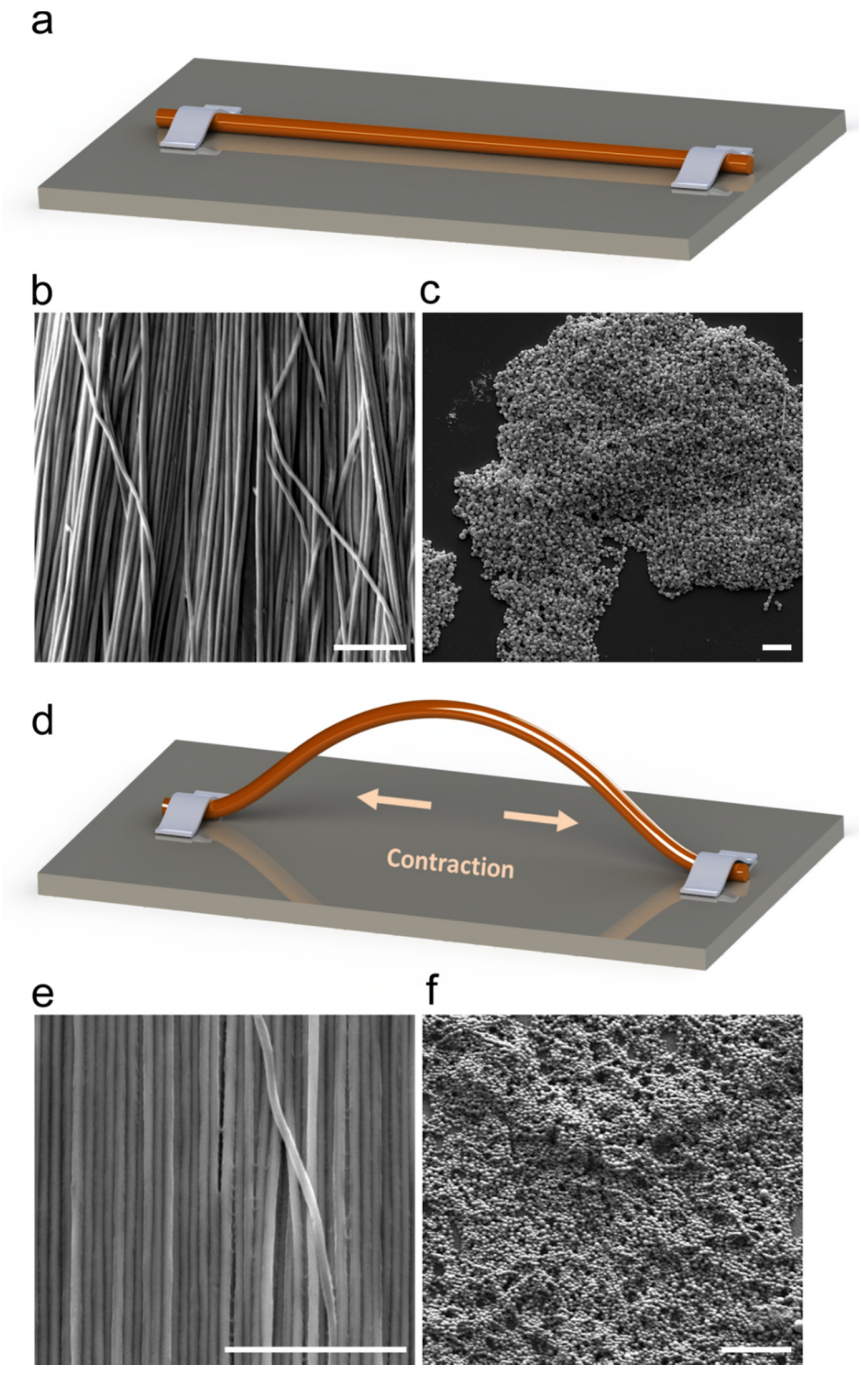

Figure S5| "Taut" and "slack" fabrication. a-c, "Taut" fibers produce nanospheres with average diameters (500 nm) similar to that of the initial nanowire (450 nm). **d-f**, "Slack" fibers, in contrast, produce much wider diameters due to the thermal contraction of the fiber, yielding nanospheres with an average diameter of 400 nm from 200 nm core-shell nanowires. All scale bars, 5 µm.

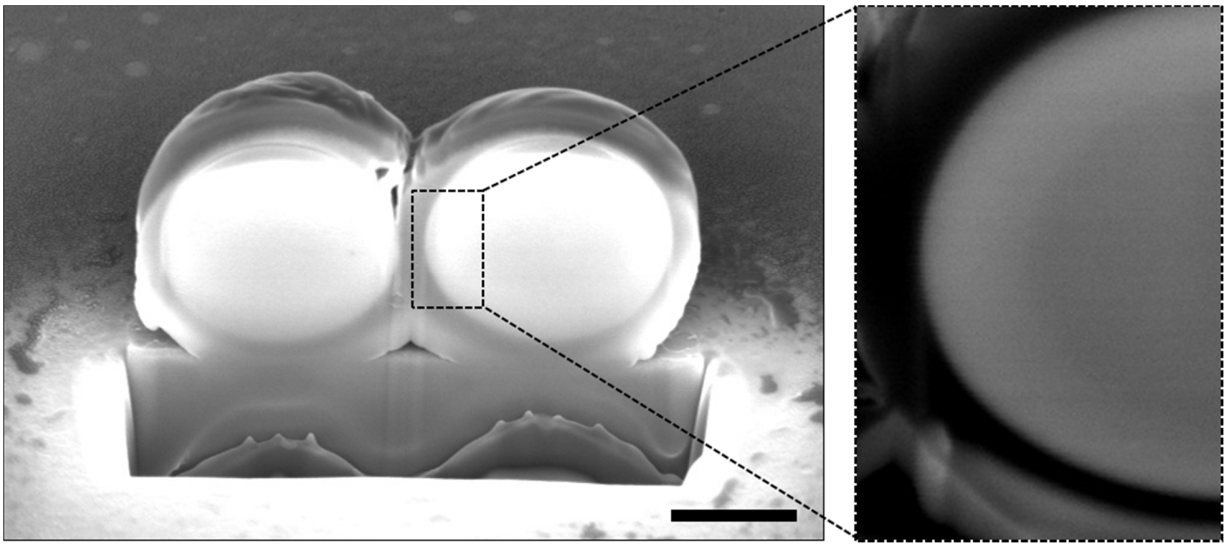

Figure S6| The uniformity of structures. Two microchain links exhibit smooth surfaces and no apparent irregularities, even under high magnification. Scale bar, 1 µm.

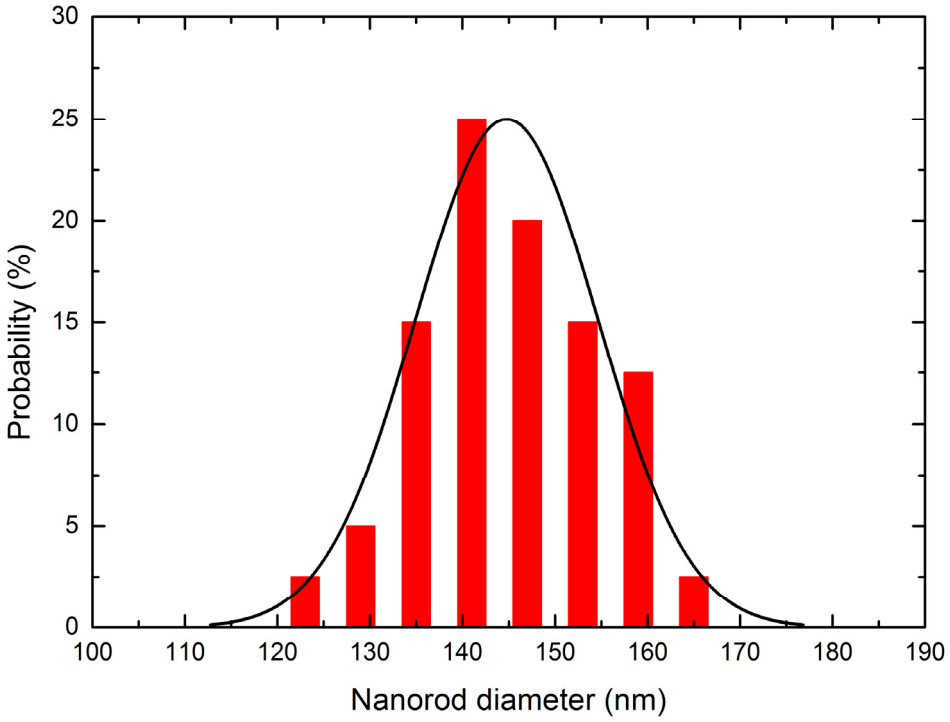

Figure S7 | Size distribution of fabricated nanostructures. Radial size distribution of fabricated nanoschemes possess consistent structural dimensions with low dispersion in size. The size distribution histogram of shell-embedded nanorods yield a standard deviation to diameter ratio of σ/d=%7. Similar results also observed in other nanostructures. The fact that our colored nanostructure arrays display highly uniform hue (*see* Figure 6) should also attest to the fact that the produced nanostructures are highly regular and do not display large batch variations in size, as a broad size distribution would have caused significant color shifts in colored arrays.

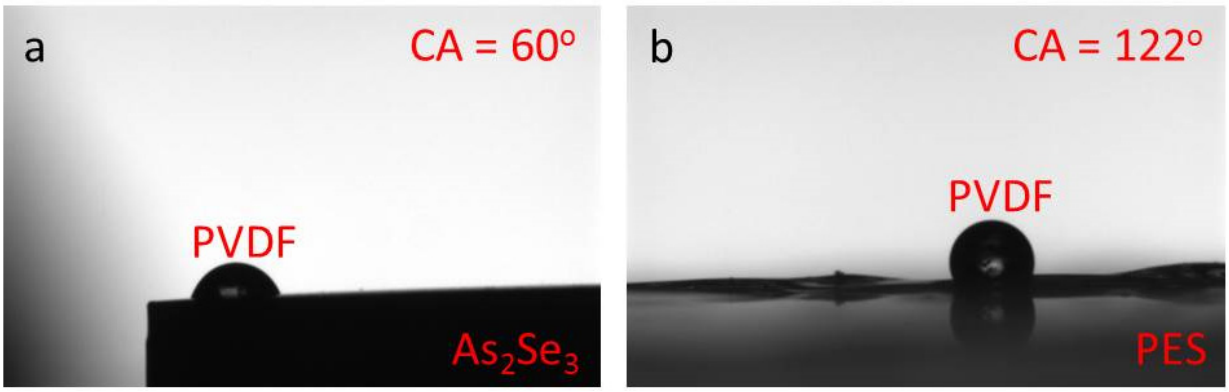

Figure S8 | Surface energy of interfaces. Contact angle (CA) measurements are performed for PVDF drop on **a**, As_2Se_3 surface and **b**, PES surface cases. Process temperature set to T=260 °C for a long duration (t=60 min) in order to minimize effect of PVDF viscosity (melting temperature for PVDF polymer is around T=175 °C). PVDF forms a contact angle of 122° with PES, which is double of that of PVDF-glass interface. Hence, PVDF-glass surface observed to has less interfacial energy than PVDF-PES surface.

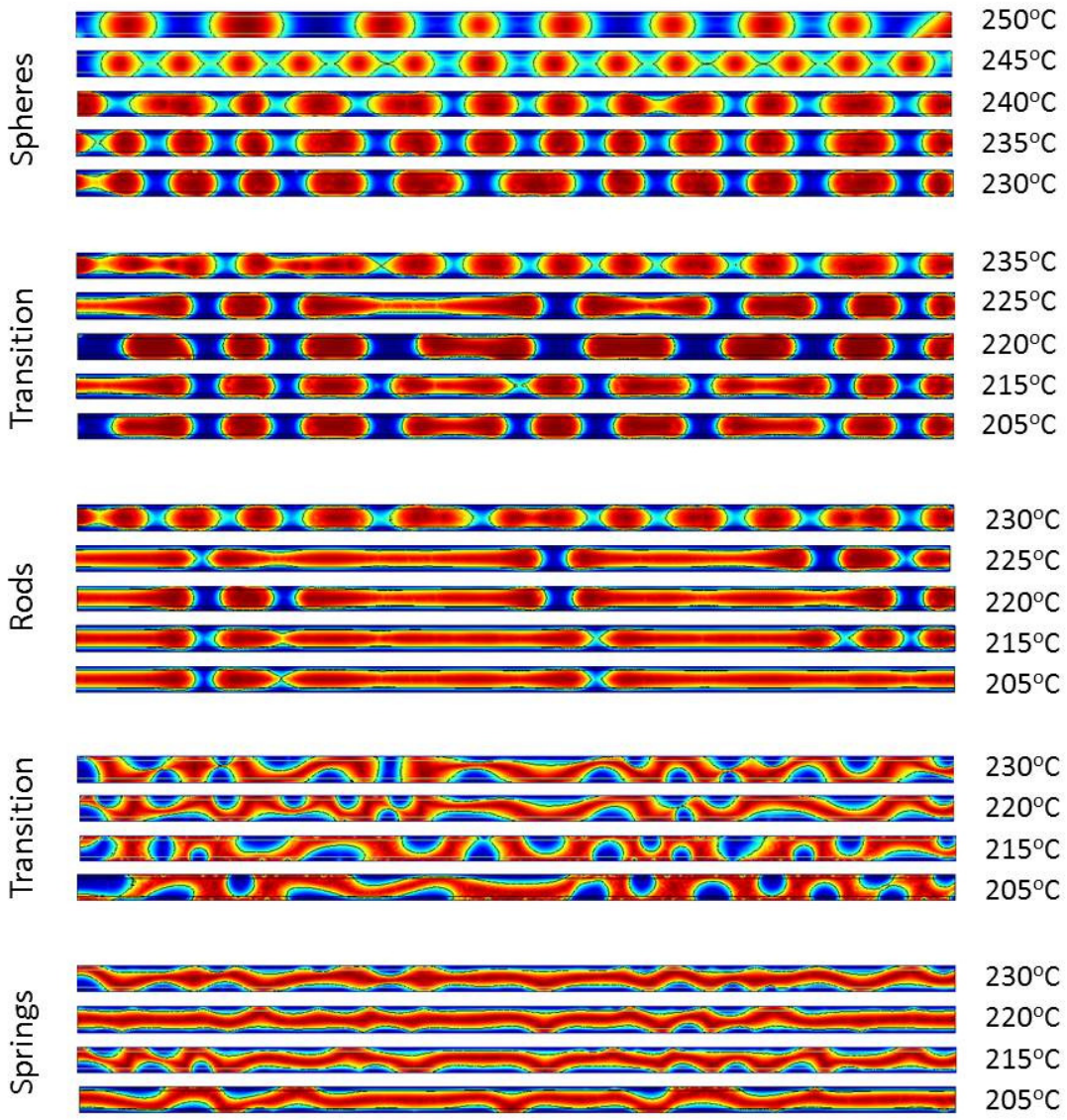

Figure S9 | Fluid dynamic simulation results. Snap-shots from simulation movies are used for the construction of the phase diagram which depict formation conditions (temperature and duration) for the springs, rods and spheres in addition to the transition regions inside of 5 µm long wires. Measured contact angle (CA = 122 °) (obtained for liquid PVDF on PES case) is used as a boundary condition in our simulations (see Figure S7). This angle is valid only when measurement is performed in air. However, after spiral formation, the third environment becomes As_2Se_3 instead of air. To avoid this problem, we design the simulations with the contact angle boundary conditions for the springs and non-slip boundary condition for the rods and spheres.

Figure S9 shows the results of our simulation at temperatures T = 205, 215 and 230 °C. The simulation at low temperature (T = 205 °C) resulted in spiral deformation of the PVDF-covered glass core, which agrees with the experimentally observed phenomenon (3b). Increasing the temperature to 215°C decreases the viscosity of the glass core and hence accelerates the process of spiral formation, which eventually culminates in the fractionation of the core. Our simulation predicts that rod formation should occur after prolonged time periods, and that these rods should display varying edge shapes (unlike our experimental results, cf. Fig. 3c). The reason for this discrepancy is that our simulation uses the experimentally determined contact angle between PVDF and PES as determined experimentally (CA = 122 °), which is only valid when measured in air. However, after spiral formation, the third environment is As_2Se_3 instead of air, which renders the simulation inadequate for predicting rod edge shapes. To avoid this problem, we use the solution at t = 500s and continue the simulation using a different PVDF-PES boundary condition. Figure 4 shows that the break-up proceeds and rods start to form after t = 700 s, and appear in full at t = 1000s,1000 s and stay stable for up to 600 s. At a more elevated temperature of T = 230 °C, the spiral formation takes place 10 times faster than it does at 215 °C. However, the experimentally observed sphere formation cannot be obtained by the simulation due to two reasons: The first reason is the boundary condition change, as in the previous case. The second reason is that this simulation assumes that PES is still solid and forms a rigid wall. This is not the case at T = 230 °C, which is higher than the glass transition temperature of PES (T_g = 220 °C). If the boundary conditions are changed, our T = 230 °C simulation predicts that rods should form at t = 100s (as opposed to 1000s at T = 215 °C). After the formation of distinct, polymer-embedded viscous As_2Se_3 rods, surface tension will cause the formation of spheres. Because the surface energy of the interface between PVDF-As_2Se_3 (σ = 0.012 N/m) is less than that of PES-As_2Se_3 (σ = 0.1 N/m),[2], PVDF prefers to enclose As_2Se_3 and core-shell spheres form. In addition, we notice

[2] Shabahang, S., Kaufman, J. J., Deng, D. S. & Abouraddy A. F. Observation of the Plateau-Rayleigh capillary instability in multi-material optical fibers. Appl. Phys. Lett. 99, 161909 (2011).

that by increasing the temperature, the axial shift between the interface perturbation peaks decreases. The main reason of this axial shift is the viscosity of the core. Increasing the temperature reduces the core viscosity and hence reduces the shift. If this shift reaches zero, the axisymmetric condition is valid and necking starts to occur. In addition, we perform the simulation of the rods and spheres formation for 5 μm long wires to demonstrate the long-term nanostructures, as shown in Figure S9.

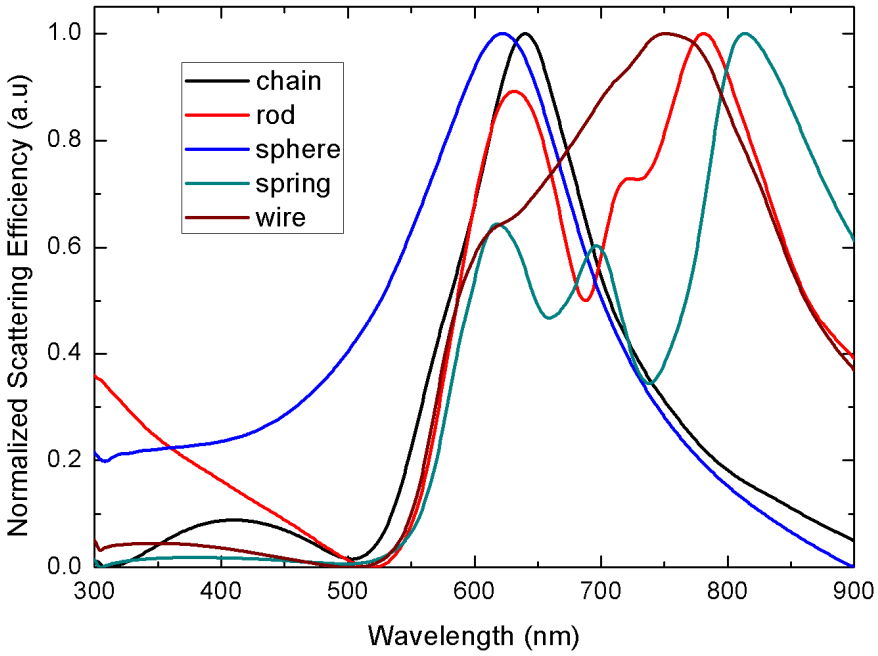

Figure S10 | Scatterings from various nanostructured morphologies. Scattering profiles of each fabricated scheme is obtained by using FDTD simulation for nanostructure diameters of 200 nm. The use of real ellipsometric constants results in the disappearance of higher modes, especially in lower wavelengths where scattering is hindered by absorption by the As_2Se_3 core. Structure lengths are 3 µm for each scheme. 250 nm rods with interstructural distances of 200 nm were utilized for discrete rod simulations. While all fabricated nanostructures are expected to yield a red-orange color at 200 nm, pronounced differences are present in their scattering characteristics.